Earth and Space Science

RESEARCH ARTICLE
10.1029/2022EA002456

Missing Rainfall Extremes in Commercial Microwave Link Data Due To Complete Loss of Signal

Julius Polz[1], **Maximilian Graf**[1,2], **and Christian Chwala**[1,2]

[1]Institute of Meteorology and Climate Research, Karlsruhe Institute of Technology, Campus Alpin, Garmisch-Partenkirchen, Germany, [2]Chair of Regional Climate and Hydrology, Institute of Geography, University of Augsburg, Augsburg, Germany

Abstract An important aspect of rainfall estimation is to accurately capture extreme events. Commercial microwave links (CMLs) can complement weather radar and rain gauge data by estimating path-averaged rainfall intensities near ground. Our aim with this paper was to investigate attenuation induced complete loss of signal (blackout) in the CML data. This effect can occur during heavy rain events and leads to missing extreme values. We analyzed 3 years of attenuation data from 4,000 CMLs in Germany and compared it to a weather radar derived attenuation climatology covering 20 years. We observed that the average CML experiences 8.5 times more blackouts than we would have expected from the radar derived climatology. Blackouts did occur more often for longer CMLs (e.g., >10 km) despite their increased dynamic range. Therefore, both the hydrometeorological community and network providers can consider our analysis to develop mitigation measures.

Plain Language Summary Commercial microwave links (CMLs) are used to transmit information between towers of cellphone networks. If there is rainfall along the transmission path, the signal level is attenuated. By comparing the transmitted and received signal levels, the average rainfall intensity along the path can be estimated. If the attenuation is too strong, no signal is received, no information can be transmitted and no rainfall estimate is available. This is unfavorable both for network stability and rainfall estimation. In this study, we investigated the frequency of such blackouts in Germany. How many blackouts per year are observed in a 3 year CML data set covering around 4,000 link paths and how many are expected from 20 years of weather radar data? We observed that the average CML experiences 8.5 times more blackouts than we would have expected from the radar derived climatology. Blackouts did occur more often for long CMLs, which was an unexpected finding. While only one percent of the annual rainfall amount is missed during blackouts, the probability that a blackout occurs was very high for high rain rates. Both, the hydrometeorological community and network providers can consider our analysis to develop mitigation measures.

Julius Polz and Maximilian Graf are shared first authorship.

Key Points:

- Complete loss of commercial microwave link (CML) signals during heavy rain leads to missing rainfall extremes
- Magnitude of observed blackouts exceeds climatologically expected values
- Unexpectedly, longer CMLs experience more blackouts

Correspondence to:
J. Polz and M. Graf,
julius.polz@kit.edu;
maximilian.graf@kit.edu

Citation:
Polz, J., Graf, M., & Chwala, C. (2023). Missing rainfall extremes in commercial microwave link data due to complete loss of signal. *Earth and Space Science*, *10*, e2022EA002456. https://doi.org/10.1029/2022EA002456

Received 7 JUN 2022
Accepted 13 JAN 2023

Author Contributions:
Conceptualization: Julius Polz, Maximilian Graf, Christian Chwala
Data curation: Julius Polz, Maximilian Graf, Christian Chwala
Formal analysis: Julius Polz, Maximilian Graf
Funding acquisition: Christian Chwala
Investigation: Julius Polz, Maximilian Graf
Methodology: Julius Polz, Maximilian Graf, Christian Chwala
Resources: Christian Chwala
Software: Julius Polz, Maximilian Graf, Christian Chwala
Supervision: Christian Chwala
Validation: Julius Polz, Maximilian Graf
Visualization: Julius Polz, Maximilian Graf

1. Introduction

Microwave radiation is attenuated by hydrometeors through scattering and absorption processes. For raindrops an advantageous relationship between specific attenuation k in dB km^{-1} and rainfall rate R in mm hr^{-1} exists. This power law known as the k-R relation is close to linear at frequencies between 20 and 35 GHz (Chwala & Kunstmann, 2019). Commercial microwave links (CMLs) use frequencies from 7 to 80 GHz and thus can be used to derive path averaged rainfall intensities by comparing transmitted and received signal levels (*TSL* and *RSL*) (Uijlenhoet et al., 2018). In theory, the k-R relation is valid for arbitrary rainfall intensities occurring in the underlying drop size distribution simulations. In practice, the measurement of high attenuation values at a given transmitted signal level has an upper bound when the signal cannot be distinguished from the receiver's background noise.

CML rainfall estimates were derived for many countries around the globe, for example, the Netherlands (Overeem et al., 2016), Sri Lanka (Overeem et al., 2021), Burkina Faso (Doumounia et al., 2014) and Germany (Graf et al., 2020). CML-derived rainfall information can be used for applications like streamflow prediction, urban drainage modeling, agricultural purposes and rainfall nowcasting (Brauer et al., 2016; Fencl et al., 2013; Imhoff et al., 2020; Stransky et al., 2018). Especially for flash flood prediction, precise precipitation maxima are of great importance (Cristiano et al., 2017). While rainfall estimates from weather radars are known to underestimate high intensities (Schleiss et al., 2020), rain gauges lack spatial representativeness (Sevruk, 2006). CMLs can fill this information gap by estimating path averaged intensities at path lengths of a few kilometres.

Writing – original draft: Julius Polz, Maximilian Graf
Writing – review & editing: Julius Polz, Maximilian Graf, Christian Chwala

Recent studies on the quality of CML rainfall estimates suggest a good agreement with radar and rain gauge estimates (Graf et al., 2021; Overeem et al., 2021). However, missing periods in the signal level time series might be excluded for example, when comparing CML time series against a path-averaged radar reference or rain gauges. Such periods can occur due to hardware failure, maintenance or outages in the data acquisition. Additionally, network providers usually design the hardware in such a way that transmission outages due to high attenuation (blackouts) are allowed to occur for a certain amount of time per year. The International Telecommunication Union (ITU) recommends a minimum availability of 99.99% which would allow up to 52 min of complete loss of signal per year (ITU-R, 2017).

Rainfall is the prevalent reason for CML signal attenuation. Hence, the amount of missing data is in a close relationship with the local rainfall climatology. Because of blackouts rainfall estimates from CMLs miss peak intensities, an error which propagates to further applications. Figures 1a–1d shows examples of such blackouts in CML attenuation time series and the rainfall intensity according to a weather radar reference. To date, it is unclear to what extent rain events are missed due to blackouts.

Our aim is to answer two questions related to CML blackouts using a country-wide CML network in Germany. The first question is how many blackouts each CML is experiencing in practice and how this affects rainfall estimates. The second question is how much blackout time is expected considering a 20 year high-resolution weather radar rainfall climatology and how this expectation compares to the results derived from the CML data.

2. Data and Methods

Our analysis was based on observed blackouts within CML data collected in Germany and a comparison to the expected frequency derived from weather radar climatology (Section 2.1). We detected gaps in CML data that are assumed to be caused by attenuation (Section 2.2) and derived path integrated attenuation (PIA) values from path averaged weather radar rain rates (Section 2.3). Note that all calculations were repeated for each CML individually.

2.1. Data

CML data has been collected in cooperation with Ericsson Germany. The data acquisition system described by Chwala et al. (2016) has been used to record 3 years of instantaneously measured *RSL* and *TSL* of 3,904 CMLs distributed over Germany (2018–2020). The temporal resolution is 1 min and the power resolution is 0.3 or 0.4 dBm for *RSL* and 1 dBm for *TSL*. 25% of the CMLs have a constant *TSL* value (e.g., Figure 1b). The other 75% use an automatic transmit power control, which can increase *TSL* if *RSL* decreases due to attenuation (e.g., Figures 1a, 1c, and 1d). The CML path lengths range from 0.1 to 30 km with frequencies from 7 to 40 GHz as shown in Figure 2d. In the context of rainfall estimation, CMLs are characterized by two main features. First, the signal level sensitivity to rainfall, see for example, Figure 7 in Chwala and Kunstmann (2019), which depends on the frequency, polarization and path length. Second, the dynamic range of the signal level D_{range}, that is, the difference between clear sky attenuation and maximum measurable attenuation. The communication along a CML requires (de-)modulation of information onto the carrier frequency. Different modulation schemes are used. In case of increased attenuation along their path, the CMLs switch to more simple modulation. This decreases the useable bandwidth but increases the robustness against transmission errors stemming from the lower signal-to-noise ratio during attenuation events (Bao et al., 2015). If the *RSL* is too low, that is, close to the noise floor of the receiver, the error rate for demodulation becomes too large and communication is cut off. Datasheets of CML hardware (e.g., from Ericsson (2012)) guarantee a certain error rate at defined low *RSL* values rather than a fixed lower *RSL* limit where this cutoff happens. Therefore, we need to estimate the empirical D_{range} of each CML as

$$D_{range} = TSL_{max} - RSL_{min} - TSL_{min} + RSL_{max}. \quad (1)$$

We removed *TSL* and *RSL* outliers outside the intervals (−20, 50 dBm) and (−99, 0 dBm) respectively. TSL_{max} and RSL_{min} were the highest (lowest) values which occurred during heavy attenuation events representing the strongest observed attenuation event for each single CML (see Figures 1a–1d as examples). Contrarily, we can assume that TSL_{min} and RSL_{max} are occurring frequently during clear sky conditions. To account for individual outliers we removed values for TSL_{min} and RSL_{max} when they occurred less often than approximately 1 hr in total during the

10.1029/2022EA002456

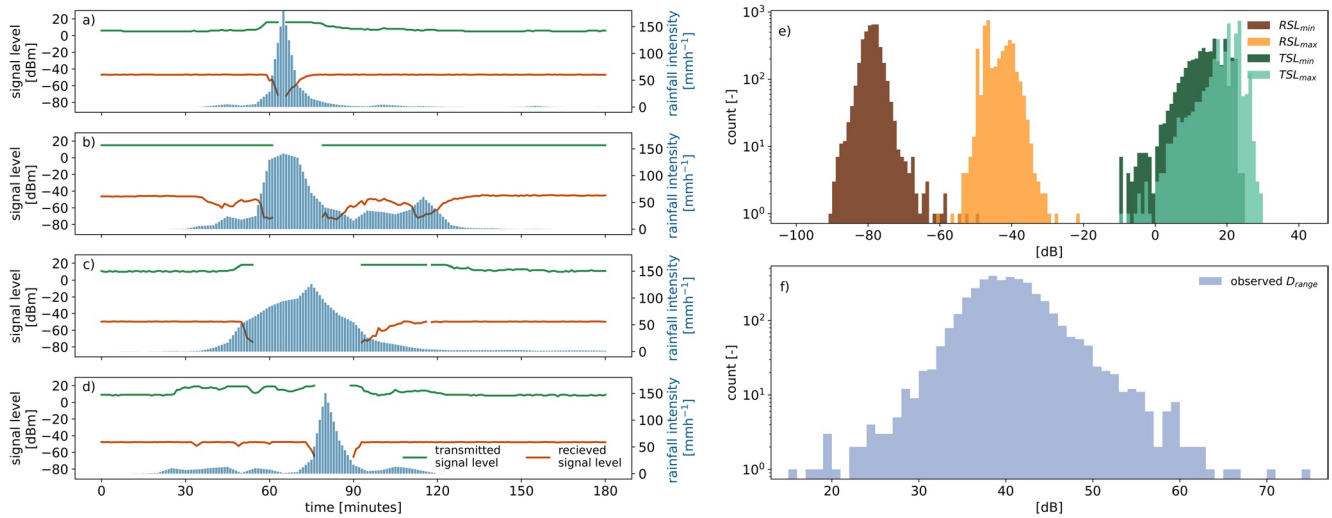

Figure 1. (a–d) show *TSL* and *RSL* time series during blackout gaps from four commercial microwave links (CMLs). Rainfall intensities are derived from RADKLIM-YW along the CML's paths. (e) gives the minimal and maximal *TSL* and *RSL* values of all 3,904 CMLs for the analyzed period of 3 years. (f) shows the distribution of the dynamic range directly calculated from CML signal levels with Equation 1.

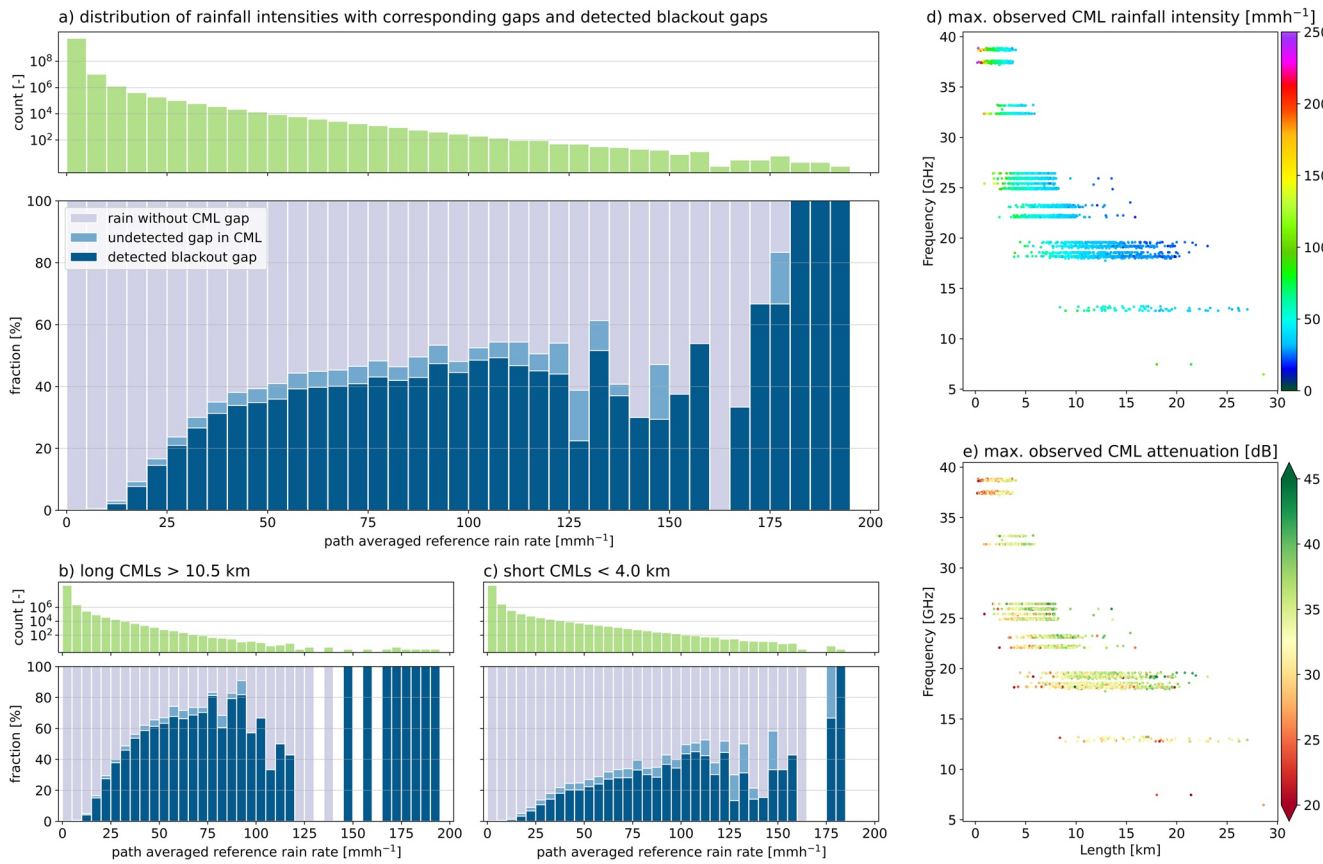

Figure 2. (a) shows the distribution of the reference rainfall intensities in green. For each bin the fraction of gaps in the commercial microwave links (CMLs) *RSL* time series and the fraction of the detected blackout gaps are shown in light and dark blue. (b and c) show the same for the longest (>10.5 km) and shortest (<4.0 km) quartile of all CMLs, respectively. Note that gaps that were attributed to, for example, failure of the data acquisition, have been removed as described in Section 2.1 for (a, b, and c). (d) shows the maximal rainfall intensity derived from the CMLs estimated with the rainfall retrieval methodology from Graf et al. (2020) and Polz et al. (2020). (e) shows the respective maximal attenuation observed at each CML during the analyzed 3 years.

3 years, that is, using the 99.995% quantile. Without this filter D_{range} would be overestimated for about half of all CMLs because there are individual rarely occurring high RSL_{max} or low TSL_{min} values.

With the potentially abrupt onset of heavy rainfall causing a complete loss of signal, RSL_{min} may have been undersampled by the 1-min instantaneous data sampling. Therefore, the derived D_{range} can be assumed to be the minimal dynamic range a CML has.

As reference we used RADKLIM-YW (Winterrath et al., 2018) from the German Meteorological Service Deutscher Wetterdienst which we linearly interpolated from a 5- to a 1-min resolution to match the CML resolution. RADKLIM-YW is a gauge-adjusted, climatologically corrected radar product with a temporal resolution of 5 min and a spatial resolution of 1 km. The underlying radar precipitation scans have been carried out every 5 min. Therefore, the radar rainfall intensities can be considered to be instantaneous measurements without temporal averaging. The product is composed of 17 weather radars and adjusted by more than 1,000 rain gauges with additive and multiplicative corrections. The climatological correction accounts for range-dependent underestimation and radar spokes caused by beam blockage, among others. RADKLIM-YW was considered the best and highest resolved rainfall reference for this analysis and was available from 2001 to 2020. Following Graf et al. (2020) we derived the path averaged rain rate R for each CML as the sum of radar grid cell rainfall intensities r_i weighted by their lengths of intersection l_i with a given CML path of total length L as described by Equation 2.

$$R = \frac{1}{L}\sum_i r_i l_i \tag{2}$$

To be able to investigate a potential temperature dependence of observed blackouts we used the 2 m temperature from the ERA5 analysis data set provided by the European Centre for Medium-Range Weather Forecasts (Muñoz-Sabater et al., 2021). The temporal resolution is instantaneous at a 1 hr frequency and the spatial resolution is 9 km. Similar to Equation 2 an average along the CML path was computed by a weighted sum of ERA5-land grid cells intersected by the CML path.

2.2. Detecting Blackouts in CML Data

Gaps in CML signal level time series can have various causes. In this analysis we were interested in gaps caused by strong attenuation during heavy rainfall and therefore excluded periods which could be attributed to one of the following causes. Gaps longer than 24 hr were assumed not to be caused by heavy rain events. When more than 400 CMLs exhibited a gap at the same time, we excluded this time step. The reasoning behind this value is that we assumed a partial or complete outage of our data acquisition system which polls the data in several batches of 400–500 CMLs every minute. Gaps occurring during a period where a seven-day rolling mean of the *RSL* was below −60 dBm were removed. This was done, because we can assume that there is a long-term transmission disturbance, that is, partial beam blockage due to a growing tree or due to ice cover on the antenna during consecutive winter days with temperatures below freezing point, since none of the CMLs in our data set has a 3-year median *RSL* below −60 dBm. That is, all our CMLs have their long-term baseline *RSL* level during clear sky conditions above −60 dBm. Around 0.2% of all *RSL* values are removed from the analysis by filtering data acquisition gaps and long term transmission disturbances.

The actual detection of blackout gaps is done with the remaining CML data based on the following rule. A gap is defined as a blackout gap if either the last valid *RSL* before, the first valid *RSL* after this gap, or both values were below −65 dBm. Examples of such automatically detected gaps are shown in Figures 1a–1d. The median *RSL* levels within our data set are well above −65 dBm. Therefore, we chose this threshold to select only events with attenuation typical for heavy rain events. The thresholds we chose for filtering the data and detecting the blackout gaps proved to be robust when applied to our data set where the CML hardware and data acquisition are homogeneous (Chwala et al., 2016). However, they might need adjustment if our method is applied for CML data sets with different characteristics.

We grouped observed blackouts into reference rainfall intensity bins and computed the average amount of observed blackout minutes n_{obs} per year for each CML. In addition, n_{obs} was normalized by applying the factor

$$f_{avail} = \frac{\#\{\,minutes\ in\ observation\ period\,\}}{\#\{\,minutes\ with\ valid\ observations\,\}} \tag{3}$$

for each CML to account for missing time steps in the CML data.

2.3. Deriving a Blackout Climatology From Radar Data

In theory, a blackout due to heavy rainfall should be expected whenever the PIA exceeds the CML's dynamic range D_{range}. We estimated a blackout climatology using 20 years of instantaneous radar measurements. A radar derived PIA was calculated by individually applying the k-R relation to the rain rate r_i of the ith radar grid cell intersected by a CML path. This procedure was chosen over applying the k-R relation to the path averaged rain rate to minimize errors due to the spatial variability of rainfall along the path as explored by Berne and Uijlenhoet (2007). Hence, we calculated

$$PIA = \frac{1}{L}\sum_i a r_i^b l_i + w_{aa} \tag{4}$$

using coefficients a and b, derived from the ITU recommendation ITU-R (2005), which depend on the CMLs frequency and polarization. The intersection length of CML path and radar grid cell i is denoted l_i. Additionally, a constant $w_{aa} = 3$ dB accounting for the wet antenna attenuation (WAA) caused by rain drops on the cover of the CML antennas was added (van Leth et al., 2018). We chose a value similar to Leijnse et al. (2008); Schleiss et al. (2013). We assumed a high constant value which is reasonable for peak rainfall intensities. Whenever PIA was larger than D_{range}, the CML was expected to show a blackout gap. Thus, we derived the cumulative number of expected blackout minutes $n_{\exp}(D_{range})$ as the average number of timestamps per year where PIA > D_{range} multiplied by five due to the radar's instantaneous sampling rate of 5 min. We applied Equation 3 to $n_{\exp}$ according to the radar availability along CML paths. Due to RSL_{min} undersampling, D_{range} might be higher in reality than estimated. In turn, $n_{\exp}$ should be lower than estimated, that is, we would expect n_{obs} to be smaller than $n_{\exp}$.

3. Results

3.1. CML Signal Levels and Dynamic Ranges

The distribution of TSL_{min} and TSL_{max} is defined by hardware configuration. The distribution of RSL_{min} and RSL_{max} depends on TSL, path length and path loss. The spread of observed RSL_{max} is lower than the spread of observed RSL_{min}. The distribution of the dynamic range estimate is shown in Figure 1f. The observed D_{range} was on average 40.5 dB with a minimum of 15.2 dB and a maximum of 74.3 dB.

3.2. Observed CML Blackout Gaps

Figure 2a shows a histogram of path-averaged radar rainfall intensities. The higher the path-averaged rainfall intensity the less frequently it occurred. For each bin the fraction of CML data gaps which were detected as blackout gaps are shown (dark blue). In addition, the fraction of all gaps that have not been detected as blackout are shown (light blue). Note that gaps that were attributed to, for example, failure of the data acquisition, have been removed as described in Section 2.1. The fraction of gaps is increasing quickly until 50 mm hr^{-1} and then less steep up to 125 mm hr^{-1}. For very high intensities above 125 mm hr^{-1} the sample size was less than 50 min per bin. Therefore, the fraction of all gaps, including detected blackout gaps, was becoming sensitive to the occurrence of individual events and hence the statistics were less robust. Overall, around 95% of the gaps during rainfall in the radar reference were detected as blackout gaps. This fraction varied for the highest observed rainfall intensities due to the small sample size. Based on the statistics from Figure 2a, CMLs missed on average 1% of the yearly rainfall sum during blackout gaps.

The quartile of long CMLs, that is, longer than 10.5 km, in Figure 2b showed a higher fraction of (blackout) gaps. Additionally, path-averaged rainfall intensities are lower on average as longer paths average out peak intensities. The quartile of short CMLs, that is, shorter than 4.0 km, shows fewer (blackout) gaps and higher rainfall intensities. This pattern is also visible in Figures 2d and 2e) where the maximum instantaneous rainfall intensity and attenuation from each CMLs observations are shown. While the maximum attenuation increased with length, the maximum observed path-averaged rainfall intensity decreased. The maximum observed rainfall intensity from CMLs with 600 mm hr^{-1} (and several events above 250 mm hr^{-1} all beyond the figures colorscale) is well above the maximum intensity of the path averaged reference product. Overall, shorter CMLs show fewer blackouts during heavy rainfall.

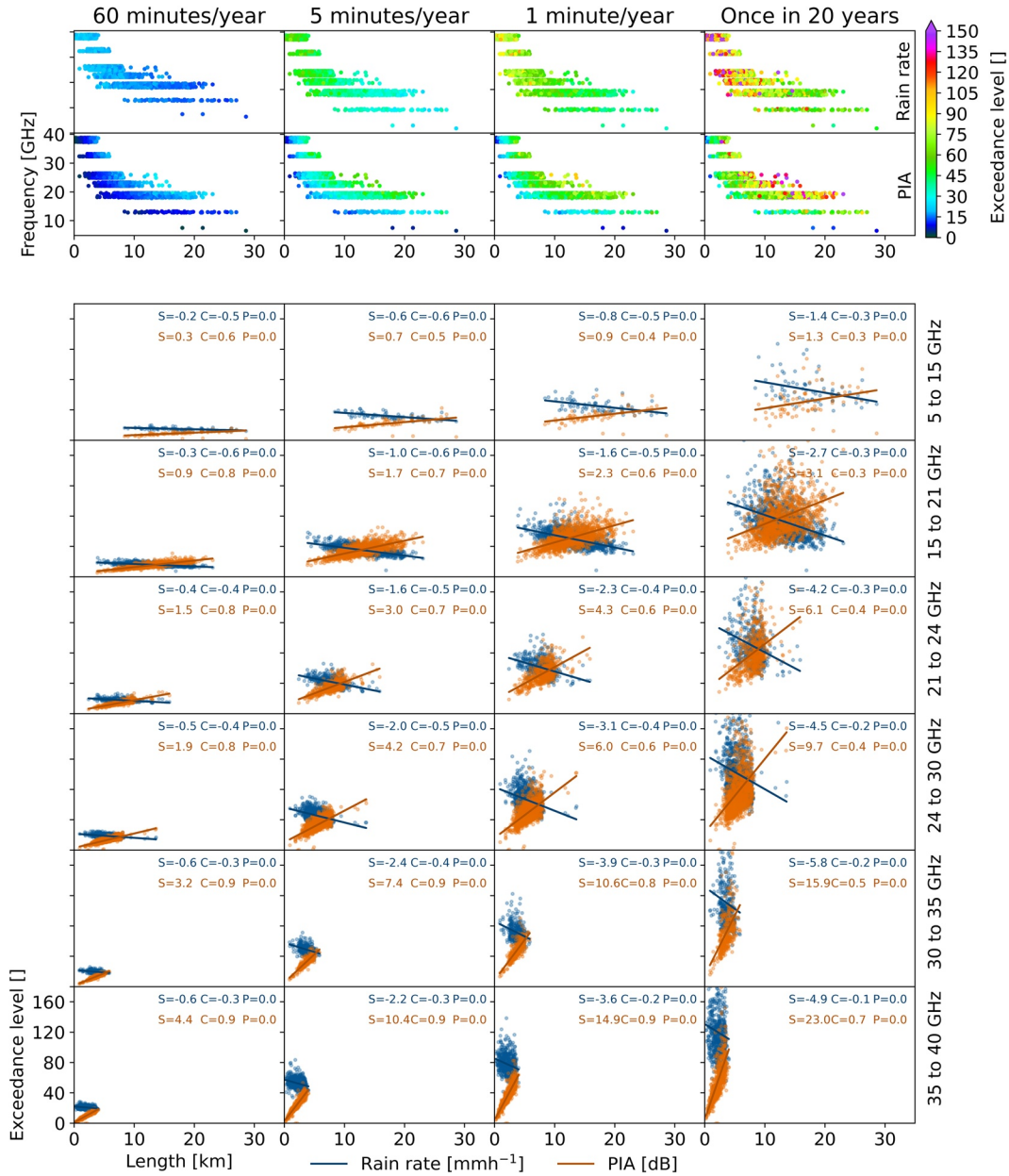

Figure 3. Rainfall and attenuation climatology for individual commercial microwave links (CMLs) based on 20 years of RADKLIM-YW. The exceeded path-averaged rain rate and path integrated attenuation (PIA) along each CML path of a given length and frequency for at least 60, 5, and 1 min per year and the maximum rain rate occurring once in 20 years are shown in the four columns. The top two rows show rain rate and PIA (same color scale) as length against frequency scatterplots. Below, the same rain rate and PIA exceedance levels are compared to the CML length data points shown for six frequency bins. The respective linear regression lines are shown with values for slope (S), correlation (C) and *p*-value (P).

3.3. Expected Blackout Gaps Derived From Radar Based Attenuation Climatology

Expected PIA values along each CML path were derived using Equation 4 and 20 years of RADKLIM-YW data. Figure 3 shows path-averaged rain rate and PIA percentiles of the full 20-year data set corresponding to the highest 60, 5 or 1 min per year and the 20-year maximum for individual CMLs (i.e., 60 min per year corresponds to the highest 0.011415526% in the data). The expected PIA was increasing with CML length, while the path averaged rain rate was decreasing. The 5-min PIA exceedance level (see Figure 3 second column) was between 10 dB (first percentile), occurring mostly for shorter CMLs, and 53 dB (99th percentile), occurring

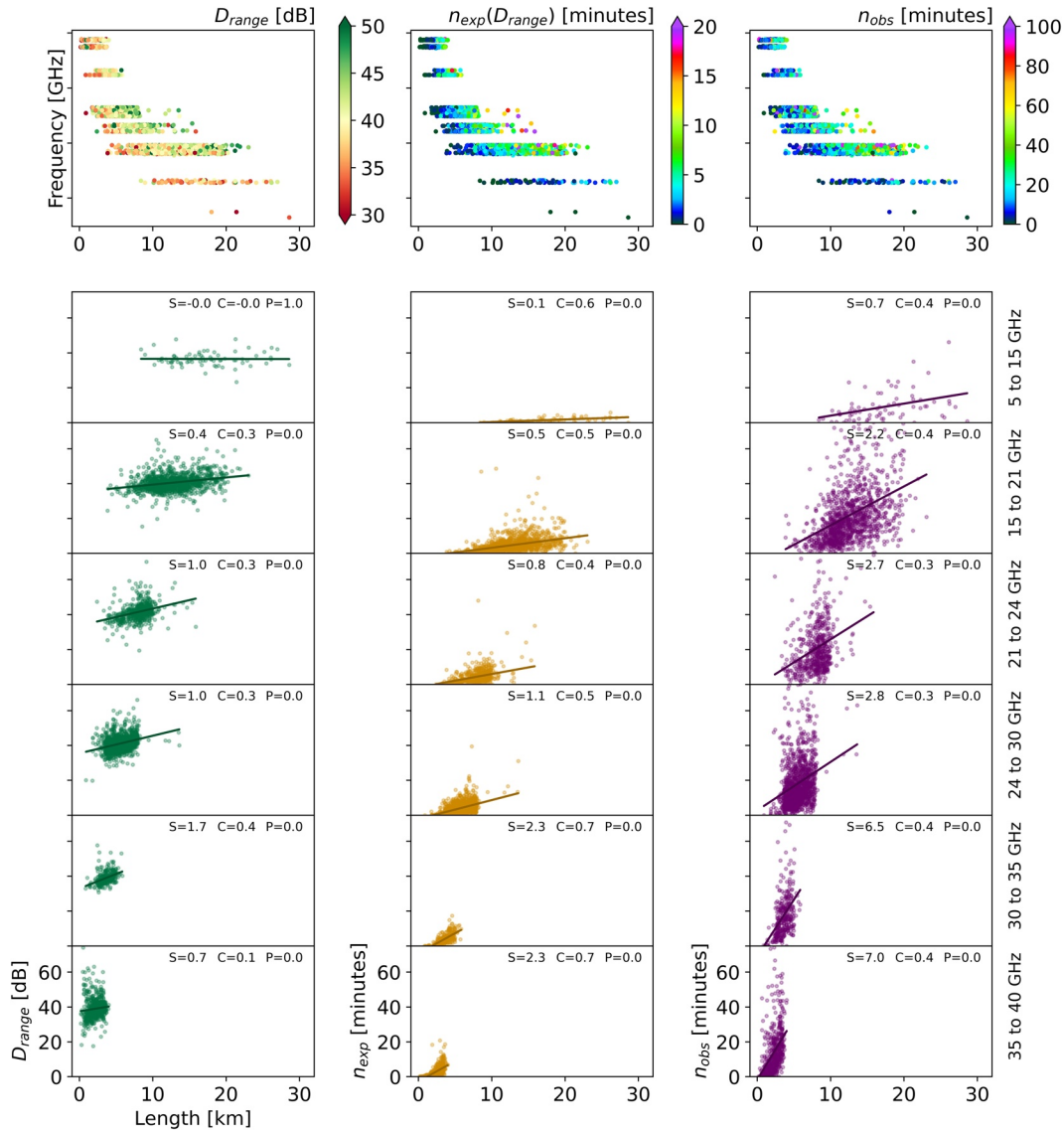

Figure 4. In the three columns D_{range} (left), n_{obs} (middle) and $n_{\exp}$ (right) are compared for each commercial microwave link (CML). The top row shows the respective variable on the color scale of a length against frequency scatterplot. Below, the three variables are shown against the CMLs length for six different frequency bins. A linear regression line and its values for slope (S), correlation (C) and *p*-value (P) is given for each of the scatter plots.

mostly for longer CMLs. On average, a path-average rain rate of 42.8 mm hr^{-1} and a PIA of 32.7 dB were exceeded for 5 min per year and a path-averaged rain rate of 17.9 mm hr^{-1} and a PIA of 13.5 dB were exceeded for 60 min per year.

The decrease of path-averaged rain rate exceedance levels with CML length was similar for all frequency bins, while the increase of PIA was higher for higher frequencies. For all frequencies, the respective de- or increase was higher for more extreme values, that is, comparing the 20-year maximum to 60 min per year, while the correlation was decreasing. The p-value was close to zero in all cases showing very high statistical significance.

Using the expected PIA values and our estimates of D_{range} we calculated $n_{\exp}$ which is shown in the second column of Figure 4. The majority of D_{range} was between 30 and 50 dB with higher values for longer CMLs (Figure 4 first column). Even though D_{range} was increasing with length, $n_{\exp}$ was also increasing with length.

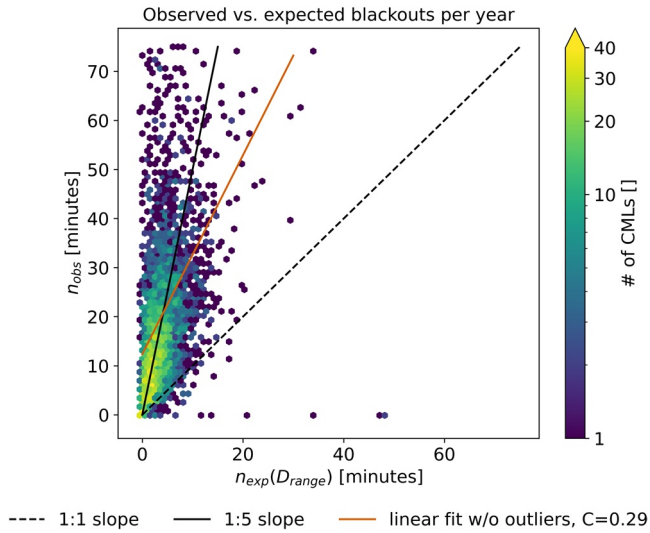

Figure 5. The observed number of blackout minutes per commercial microwave link shown is compared to the number of expected blackout minutes in the scatter density plot, where the dashed black line corresponds to a 1:1 relation and the solid black line corresponds to a 5:1 relation. The orange line shows the best linear regression fit with a slope of 2.0 and a correlation (C) of 0.29. Outliers above the 99th percentile, that is, $n_{obs} > 207.2$ or $n_{\text{exp}} > 17.5$, are excluded from the linear regression.

3.4. Comparison of Observed and Expected Blackouts

D_{range} and the number of observed (n_{obs}) and expected (n_{exp}) blackout minutes per year are shown in Figure 4 for the individual CMLs length and frequencies and shown for each length in six frequency bins. D_{range} was increasing with CML length for all frequency bins except for 5–10 GHz. We observed that n_{exp} and n_{obs} increased with CML length. However, n_{exp} showed a smaller slope than n_{obs}. The correlation between length and n_{obs} was low, but significant. The slope was strictly positive and increasing with higher frequencies, though.

Longer CMLs missed a higher percentage of high rainfall intensities than shorter CMLs (see Figures 2b and 2c). According to n_{exp} a 99.99% availability margin (as recommended by the ITU which is less than 60 min of blackouts per year) should have been observed for all CMLs. In practice, that is, for n_{obs}, the 99.99% margin (60 min) was exceeded for the longest CMLs in each frequency band. We found this to be true throughout all frequency bins except 5–15 GHz.

In Figure 5, n_{exp} is directly compared to n_{obs}. The mean of n_{obs} was 6 times higher than the mean of n_{exp}. The 99th percentiles of n_{obs} and n_{exp} were 207.2 and 17.5 min. Higher values are considered as outliers. On average n_{obs} was 12 times higher than n_{exp} for all CMLs where $n_{\text{exp}} > 0$ and 8.5 times higher if outliers were excluded. Taking the median instead of the mean, the value is 4.6 independent of outliers included or not. The average n_{obs} for CMLs where $n_{\text{exp}} = 0$ was 19.4 min and the median was 3.2 min. 95.0% of all CMLs showed more observed blackout minutes than expected, that is, $\frac{n_{obs}}{n_{\text{exp}}} > 1$. For 47.6% of the CMLs we observed more than five times more blackouts than expected and for 22.8% we observed more than 10 times more blackouts. A linear regression excluding outliers shows an additive increase of 11 min and a multiplicative increase of a factor 2. However, the correlation of 0.29 was low.

4. Discussion

4.1. Effects of CML Length on Blackout Gaps and Network Design

The result that short CMLs have a lower likeliness to experience a blackout gap than longer CMLs was unexpected, because we expected the dynamic range to increase with CML length to account for the increasing PIA. Our empirical dynamic range estimates indeed show an increase with length, but it is not sufficient to compensate the even larger increase of PIA. Also, the path-averaging effect results in lower peak intensities of the path-averaged rain rates which decreases the attenuation per kilometer of CML length.

We found this difference between short and long CMLs in both our CML data set and our radar-based attenuation climatology. Since observed and expected blackouts are based on independent methodological assumptions, we are confident that the effect is real. One potential explanation is that the path-averaging effect of peak intensities is overestimated during planning of the CMLs availability, so that longer CMLs experience more PIA than expected.

Our findings show potential to improve planning for future CML installations. Most prominently, our results suggest to increase the dynamic range of long CMLs. ITU recommends that the actual path length is multiplied by a so-called *distance factor* when calculating long-term statistics of rain attenuation ITU-R (2021). This factor significantly reduces the effective length (which is used for the calculation of path attenuation exceedance levels from rain rate exceedance statistic) of longer CMLs, for example, the factor is approximately 0.5 for a 10 km CML with 20 GHz. Our finding, that longer CMLs experience more blackouts then shorter ones, suggests that this reduction of effective length of a CML for the calculation of path attenuation statistics is too strong, resulting in longer CMLs being planned with a too low D_{range}. Our radar-based exceedance probability can be used to estimate the potential increase of blackouts with CML length on the one hand. The total number of blackouts should be expected to be much higher on the other hand, which requires an additional increase of the dynamic range for

all CMLs. As the ITU-recommended 99.99% availability was satisfied in most cases, this recommendation may be more urgent for hydrometeorological applications than network stability.

4.2. Implications of Blackouts on CML Rainfall Estimation

Previous studies which compared CML rainfall information against reference data, naturally considered blackouts as missing values and little attention was payed to their implication on CML rainfall estimation. Our results confirmed that their impact on annual precipitation sums is in fact low, with around 1%.

However, blackout gaps do impact CML-derived rainfall maps on shorter time scales and extreme value statistics in general, because extreme values are lost. The importance of this effect is illustrated by Figure 2 which shows the occurrence of blackouts during certain radar rainfall rates. The probability of a blackout at path-averaged rainfall intensities beyond 100 mm hr^{-1} is higher than 40%. To interpret such maximum observable path-averaged rainfall rates the path-averaging effect of the CML observation needs to be taken into account, which is different from point-like observations.

Since we observed that shorter CMLs have a much lower probability of blackout gaps, there cannot be a general conclusion about the capability of a CML network to capture rainfall extremes. We suggest several possibilities to deal with blackouts associated with higher rainfall estimates. For applications requiring estimates of rainfall maxima with high temporal resolution, only short CMLs could be used. Another solution could be to fill *RSL* during detected blackout gaps with the minimal observable *RSL* value. Although the true maxima cannot be recovered, this could be a reasonable first step to reduce the considerable underestimation of high rain rates in CML-derived rainfall maps.

4.3. Underestimation of Blackouts Through Radar-Based Attenuation Climatology

Our results also have potential implications for radar rainfall estimates. We observed that the average CML experienced 8.5 times more blackouts than expected from the radar-based climatology. The underestimation occurs even though our dynamic range estimate is lower than in reality due to undersampling of RSL_{min} and the consideration of 3 dB WAA. Although false positive blackout detection can not be excluded with certainty, manual checks of the blackout gap detection (see Graf et al., 2022a) confirmed the correct magnitude of observed blackouts for the vast majority of CMLs.

Therefore, there is evidence that radar-derived path-averaged rain rates and the related PIA could underestimate extreme values. This is supported by studies reporting that gauge-adjusted radar products often underestimate heavy rainfall (e.g., Schleiss et al., 2020). This underestimation could be explained by the different spatial integration characteristic of CML and radar. Another reason for the underestimation are effects that occur in combination with rainfall, for example, hail, that may lead to unexpected high attenuation values, but they may not lead to high weather radar rainfall estimates due to quality control and attenuation of the radar signal.

Melting hydrometeors like wet snow or sleet cause attenuation of CML signal larger than their rainfall equivalent (e.g., Tjelta & Bacon, 2010). We tested whether this effect influenced the number of observed blackouts by comparing blackout occurrences to the temperature along the CML paths derived from ERA5-land. Figure 6 shows the 3-year time series of daily and monthly observed and expected blackouts with the daily mean temperature from ERA5 as well as a scatter density comparison of temperature and observed blackouts occurring in 3-hr periods. Similar to van Leth et al. (2018), we assumed that almost all precipitation above 4°C is liquid. We found that 17.7% of all observed blackouts occurred below 4°C, while the majority was centered around 20°. This shows that the contribution of melting hydrometeors at temperatures below 4°C is not high enough to fully explain the underestimation of blackouts through weather radar data. It could also be observed that, as expected, blackouts rarely occur at negative temperatures. We conclude that despite the high spatial and temporal resolution, the weather radar data is not sufficient to fully explain CML blackouts.

5. Conclusions

During extreme heavy rain events, CMLs may experience blackouts, that is, complete loss of signal. Our objectives were to determine the impact on rainfall estimation, the occurrence of blackouts in a country-wide network

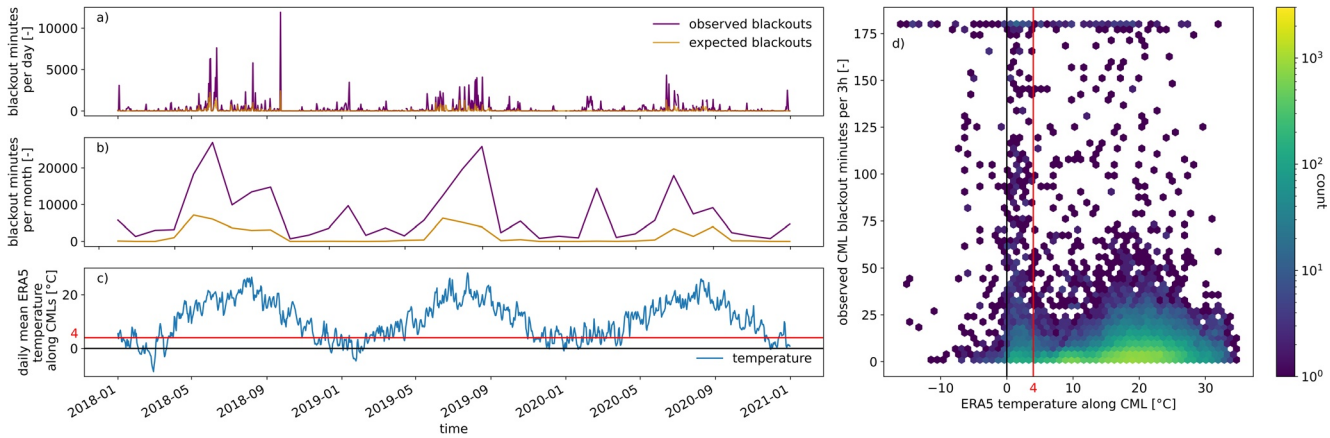

Figure 6. (a and b) show the observed and expected number of blackouts per day and month between 2018 and 2020. (c) shows the mean 2 m temperature along all commercial microwave links (CMLs) derived from ERA-5-land. (d) shows the observed number of blackout minutes per CML per 3 hr compared to the average ERA5-land 2 m temperature along the link path during the same period. The red line in (c and d) indicates the 4°C threshold below which mixed type precipitation is more likely. 17.7% of all observed blackouts occurred below this threshold.

of 3,904 CMLs and to determine if these numbers were consistent with the theoretical number of occurrences of blackouts derived from a 20-year climatology of a high-resolution weather radar product. On average, CMLs experienced 20 min of blackout per year and the average CML experienced 8.5 times more blackouts than the radar climatology suggested. Shorter CMLs showed fewer blackouts in both the observed and theoretically derived data. Although the amount of rainfall missed was small compared to annual sums, the observed probability of blackouts during path-averaged radar rainfall intensities beyond 100 mm hr^{-1} was more than 40%, which impacts CML rainfall estimates of individual heavy rainfall events on short timescales. Especially surprising was the increase of blackouts with CML length. Therefore, we suggest that the CML research community should be aware of this limitation and the proposed mitigation measures. Finally, this study fills a knowledge gap on the distribution of blackouts in CML data and weather radar derived attenuation climatology which can be considered in future CML infrastructure planning.

Data Availability Statement

Software for the blackout gap detection routine (Graf et al., 2022a) is available within the CML rainfall retrieval Python-package pycomlink (Chwala et al., 2022) under BSD-3-Clause License. The CML data supporting this research was provided to the authors by Ericsson. This data is not publicly available as Ericsson restricted the distribution of this data due to their commercial interest. In order to obtain CML data for research purposes a separate and individual agreement with the network provider has to be established. In order to allow for an independent evaluation of our methodology we published two subsets of the CML data: (a) 500 CMLs over 10 days and (b) two CMLs for the full period of this study (Chwala et al., 2022; Graf et al., 2022b) under CC BY 4.0. The RADKLIM-YW data set used in this research is publicly available and can be downloaded from Winterrath et al. (2018).

Acknowledgments
We thank Ericsson, especially Reinhard Gerigk, Michael Wahl, and Declan Forde for their support in the CML data acquisition. This research has been supported by the Helmholtz Association (Grant ZT-0025), the German Research Foundation (Grant CH-1785/1-2) and the Federal Ministry of Education and Research (Grant 13N14826). We acknowledge support by the KIT-Publication Fund of the Karlsruhe Institute of Technology. Open Access funding enabled and organized by Projekt DEAL.

References

Bao, L., Hansryd, J., Danielson, T., Sandin, G., & Noser, U. (2015). Field trial on adaptive modulation of microwave communication link at 6.8 GHz. In *2015 9th European Conference on Antennas and Propagation (EuCAP)* (pp. 1–5). IEEE. (ISSN: 2164-3342).

Berne, A., & Uijlenhoet, R. (2007). Path-averaged rainfall estimation using microwave links: Uncertainty due to spatial rainfall variability. *Geophysical Research Letters*, *34*(7), L07403. https://doi.org/10.1029/2007GL029409

Brauer, C. C., Overeem, A., Leijnse, H., & Uijlenhoet, R. (2016). The effect of differences between rainfall measurement techniques on groundwater and discharge simulations in a lowland catchment. *Hydrological Processes*, *30*(21), 3885–3900. https://doi.org/10.1002/hyp.10898

Chwala, C., Graf, M., Polz, J., Blettner, N., DanSereb, keis-f, & yboose. (2022). pycomlink/pycomlink: v0.3.5 [Software]. Zenodo. https://doi.org/10.5281/zenodo.7245440

Chwala, C., Keis, F., & Kunstmann, H. (2016). Real-time data acquisition of commercial microwave link networks for hydrometeorological applications. *Atmospheric Measurement Techniques*, *9*(3), 991–999. https://doi.org/10.5194/amt-9-991-2016

Chwala, C., & Kunstmann, H. (2019). Commercial microwave link networks for rainfall observation: Assessment of the current status and future challenges. *Wiley Interdisciplinary Reviews: Water*, *6*(2), e1337. https://doi.org/10.1002/wat2.1337

Cristiano, E., ten Veldhuis, M.-C., & van de Giesen, N. (2017). Spatial and temporal variability of rainfall and their effects on hydrological response in urban areas—A review. *Hydrology and Earth System Sciences*, *21*(7), 3859–3878. https://doi.org/10.5194/hess-21-3859-2017

Doumounia, A., Gosset, M., Cazenave, F., Kacou, M., & Zougmore, F. (2014). Rainfall monitoring based on microwave links from cellular telecommunication networks: First results from a West African test bed. *Geophysical Research Letters*, *41*(16), 6016–6022. https://doi.org/10.1002/2014GL060724

Ericsson. (2012). Receiver performance; receiver thresholds Rau1—Ericsson MINI-LINK E technical description [page 136] |ManualsLib. Retrieved from https://www.manualslib.com/manual/1620197/Ericsson-Mini-Link-E.html?page=136#manual

Fencl, M., Rieckermann, J., Schleiss, M., Stránský, D., & Bareš, V. (2013). Assessing the potential of using telecommunication microwave links in urban drainage modelling. *Water Science and Technology*, *68*(8), 1810–1818. https://doi.org/10.2166/wst.2013.429

Graf, M., Chwala, C., Polz, J., & Kunstmann, H. (2020). Rainfall estimation from a German-wide commercial microwave link network: Optimized processing and validation for 1 year of data. *Hydrology and Earth System Sciences*, *24*(6), 2931–2950. https://doi.org/10.5194/hess-24-2931-2020

Graf, M., El Hachem, A., Eisele, M., Seidel, J., Chwala, C., Kunstmann, H., & Bárdossy, A. (2021). Rainfall estimates from opportunistic sensors in Germany across spatio-temporal scales. *Journal of Hydrology: Regional Studies*, *37*, 100883. https://doi.org/10.1016/j.ejrh.2021.100883

Graf, M., Polz, J., & Chwala, C. (2022a). Blackout gap detection example notebook [Software]. Ipynb. Retrieved from https://github.com/pycomlink/pycomlink/blob/12fc302539851b19f7656cf7e2438c0ddbaa48bf/notebooks/Blackout%20gap%20detection%20examples.ipynb

Graf, M., Polz, J., & Chwala, C. (2022b). Data for a CML blackout gap detection example [Dataset]. Zenodo. https://doi.org/10.5281/zenodo.6337557

Imhoff, R. O., Overeem, A., Brauer, C. C., Leijnse, H., Weerts, A. H., & Uijlenhoet, R. (2020). Rainfall nowcasting using commercial microwave links. *Geophysical Research Letters*, *47*(19), e2020GL089365. https://doi.org/10.1029/2020GL089365

ITU-R. (2005). *Specific attenuation model for rain for use in prediction methods (Recommendation P.838-3)*. ITU-R. Retrieved from https://www.itu.int/rec/R-REC-P.838-3-200503-I/en

ITU-R. (2017). *Characteristics of precipitation for propagation modelling (Recommendation P.837-7)*. ITU-R. Retrieved from https://www.itu.int/rec/R-REC-P.837/en

ITU-R. (2021). *Propagation data and prediction methods required for the design of terrestrial line-of-sight systems* (p. 530). ITU-R. Retrieved from https://www.itu.int/rec/R-REC-P.530-18-202109-I/en

Leijnse, H., Uijlenhoet, R., & Stricker, J. N. M. (2008). Microwave link rainfall estimation: Effects of link length and frequency, temporal sampling, power resolution, and wet antenna attenuation. *Advances in Water Resources*, *31*(11), 1481–1493. https://doi.org/10.1016/j.advwatres.2008.03.004

Muñoz-Sabater, J., Dutra, E., Agustí-Panareda, A., Albergel, C., Arduini, G., Balsamo, G., et al. (2021). ERA5-Land: A state-of-the-art global reanalysis dataset for land applications. *Earth System Science Data*, *13*(9), 4349–4383. https://doi.org/10.5194/essd-13-4349-2021

Overeem, A., Leijnse, H., Leth, T. C. V., Bogerd, L., Priebe, J., Tricarico, D., et al. (2021). Tropical rainfall monitoring with commercial microwave links in Sri Lanka. *Environmental Research Letters*, *16*(7), 074058. https://doi.org/10.1088/1748-9326/ac0fa6

Overeem, A., Leijnse, H., & Uijlenhoet, R. (2016). Two and a half years of country-wide rainfall maps using radio links from commercial cellular telecommunication networks. *Water Resources Research*, *52*(10), 8039–8065. https://doi.org/10.1002/2016WR019412

Polz, J., Chwala, C., Graf, M., & Kunstmann, H. (2020). Rain event detection in commercial microwave link attenuation data using convolutional neural networks. *Atmospheric Measurement Techniques*, *13*(7), 3835–3853. https://doi.org/10.5194/amt-13-3835-2020

Schleiss, M., Olsson, J., Berg, P., Niemi, T., Kokkonen, T., Thorndahl, S., et al. (2020). The accuracy of weather radar in heavy rain: A comparative study for Denmark, The Netherlands, Finland and Sweden. *Hydrology and Earth System Sciences*, *24*(6), 3157–3188. https://doi.org/10.5194/hess-24-3157-2020

Schleiss, M., Rieckermann, J., & Berne, A. (2013). Quantification and modeling of wet-antenna attenuation for commercial microwave links. *IEEE Geoscience and Remote Sensing Letters*, *10*(5), 1195–1199. https://doi.org/10.1109/LGRS.2012.2236074

Sevruk, B. (2006). Rainfall measurement: Gauges. In *Encyclopedia of hydrological sciences*. John Wiley and Sons, Ltd. Retrieved from https://onlinelibrary.wiley.com/doi/pdf/10.1002/0470848944.hsa038

Stransky, D., Fencl, M., & Bares, V. (2018). Runoff prediction using rainfall data from microwave links: Tabor case study. *Water Science and Technology*, *2017*(2), 351–359. https://doi.org/10.2166/wst.2018.149

Tjelta, T., & Bacon, D. (2010). Predicting combined rain and wet snow attenuation on terrestrial links. In *IEEE transactions on antennas and propagation* (Vol. 58(5), pp. 1677–1682). https://doi.org/10.1109/TAP.2010.2044316

Uijlenhoet, R., Overeem, A., & Leijnse, H. (2018). Opportunistic remote sensing of rainfall using microwave links from cellular communication networks. *Wiley Interdisciplinary Reviews: Water*, *5*(4), e1289. https://doi.org/10.1002/wat2.1289

van Leth, T. C., Overeem, A., Leijnse, H., & Uijlenhoet, R. (2018). A measurement campaign to assess sources of error in microwave link rainfall estimation. *Atmospheric Measurement Techniques*, *11*(8), 4645–4669. https://doi.org/10.5194/amt-11-4645-2018

Winterrath, T., Brendel, C., Hafer, M., Junghänel, T., Klameth, A., Lengfeld, K., et al. (2018). Radar climatology (RADKLIM) version 2017.002: Reprocessed quasi gauge-adjusted radar data, 5-minute precipitation sums (YW) [Dataset]. Deutscher. https://doi.org/10.5676/DWD/RADKLIM_YW_V2017.002